

## Article

# A Progressive Plane Detection Filtering Method for Airborne LiDAR Data in Forested Landscapes

Shangshu Cai <sup>1</sup>, Xinlian Liang <sup>1,\*</sup> and Sisi Yu <sup>2,3,4</sup> 

<sup>1</sup> State Key Laboratory of Information Engineering in Surveying, Mapping and Remote Sensing, Wuhan University, Wuhan 430070, China

<sup>2</sup> Wuhan Botanical Garden, Chinese Academy of Sciences, Wuhan 430074, China

<sup>3</sup> Sino-Africa Joint Research Center, Chinese Academy of Sciences, Wuhan 430074, China

<sup>4</sup> Department of Public Administration, Law School, Shantou University/Institute of Local Government Development, Shantou University, Shantou 515063, China

\* Correspondence: xinlian\_liang@hotmail.com

**Abstract:** Ground filtering is necessary in processing airborne light detection and ranging (LiDAR) point clouds for forestry applications. This study proposes a progressive plane detection filtering (PPDF) method. First, the method uses multi-scale planes to characterize terrain, i.e., the local terrain with large slope variations is represented by small-scale planes, and vice versa. The planes are detected in local point clouds by the random sample consensus method with decreasing plane sizes. The reliability of the planes to represent local terrain is evaluated and the planes with optimal sizes are selected according to evaluation results. Then, ground seeds are identified by selecting the interior points of the planes. Finally, ground points are iteratively extracted based on the reference terrain, which is constructed using evenly distributed neighbor ground points. These neighbor points are identified by selecting the nearest neighbor points of multiple subspaces, which are divided from the local space with an unclassified point as center point. PPDF was tested in six sites with various terrain and vegetation characteristics. Results showed that PPDF was more accurate and robust compared to the classic filtering methods including maximum slope, progressive morphology, cloth simulation, and progressive triangulated irregular network densification filtering methods, with the smallest average total error and standard deviation of 3.42% and 2.45% across all sites. Moreover, the sensitivity of PPDF to parameters was low and these parameters can be set as fixed values. Therefore, PPDF is effective and easy-to-use for filtering airborne LiDAR data.

**Keywords:** ground filtering; LiDAR; forestry applications; terrain



**Citation:** Cai, S.; Liang, X.; Yu, S. A Progressive Plane Detection Filtering Method for Airborne LiDAR Data in Forested Landscapes. *Forests* **2023**, *14*, 498. <https://doi.org/10.3390/f14030498>

Academic Editor: Mark Vanderwel

Received: 29 January 2023

Revised: 12 February 2023

Accepted: 28 February 2023

Published: 2 March 2023



**Copyright:** © 2023 by the authors. Licensee MDPI, Basel, Switzerland. This article is an open access article distributed under the terms and conditions of the Creative Commons Attribution (CC BY) license (<https://creativecommons.org/licenses/by/4.0/>).

## 1. Introduction

Airborne light detection and ranging (LiDAR) can penetrate vegetation to capture accurate and detailed three-dimensional structure information of forests and is less affected by weather conditions than optical sensors [1–10]. It has become a mainstream tool in forest investigation and management [11–13].

Ground filtering, i.e., classifying ground and non-ground points, is a pre-requisite step of LiDAR data processing in many applications [14]. Therefore, various types of ground filtering methods have been developed to automatically separate LiDAR point clouds into ground and non-ground points. However, the performance of these methods is usually unreliable in forested landscapes especially containing dense vegetation and complex terrain (e.g., highly steep slopes, break lines, and ridges) [15–18]. In addition, these methods are not easy to use, because they often require tuning many parameters to achieve satisfactory results [19].

Existing ground filtering methods can be mainly categorized as slope-based [20–25], mathematical morphology-based [26–34], and surface-based methods [19,35–41]. The implementation of these three types of methods can be summarized in two steps: ground

seed (i.e., the initial ground point) identification and ground point extraction. In general, ground seeds are identified based on the feature that the ground point has the smallest height in a local region [41,42]. Ground points are iteratively extracted based on the feature that the height differences of the ground points to reference ground points or reference terrain are relatively small [43]. The slope-based methods provide an innovation to the ground point extraction step. The ground points are extracted by comparing the height differences between unclassified points and their nearest neighbor ground points (i.e., reference ground points). The threshold of height differences is set based on the maximum terrain slope in a landscape [20]. The greater the terrain slope, the greater the threshold. This innovation can reduce the risk of ground points being misclassified as non-ground points on steep slopes [44]. The mathematical morphology-based methods present an innovation in the ground seed identification step. Ground seeds are identified by selecting the lowest points within sliding windows. The window sizes are determined adaptively according to the sizes of the non-ground objects in a landscape through morphological opening operation [26,45]. The method can identify more ground seeds compared to the largest size of windows [14,16,46]. The surface-based methods propose an innovation to the ground point extraction step. Ground points are extracted by judging the height differences between unclassified points and the reference terrain constructed by neighboring ground points [35,41]. Compared to the slope-based methods, this innovation can improve filtering accuracy on undulating terrain due to the use of contextual information [14,47].

However, these methods still have some limitations when applied in forested landscapes. First, it is difficult to identify ground seeds on raised terrain, since the height of raised terrain is the local maximum [48]. The lack of ground seeds leads to poor filtering results on the terrain. Second, the window sizes in urban landscapes are usually determined by manually measuring the largest buildings. Nevertheless, the window sizes in forested landscapes are extremely difficult to be determined, because vegetation would not always be penetrated by laser pulses and the largest non-penetrated vegetation is not easily identified by users [15]. Third, the number of laser pulses penetrating vegetation to reach the ground is inconsistent due to the varying density of the canopy level, resulting in uneven ground points. The reference terrain for ground point extraction may be unreliable since the neighbor ground points searched are unevenly distributed. This also reduces the filtering accuracy.

To overcome these limitations, we propose a progressive plane detection filtering (PPDF) method, which is expected to effectively filter out non-ground points while preserving the terrain's details. Moreover, the proposed method is universally applicable, i.e., the users without much experience do not need to carefully adjust the parameters to obtain satisfactory filtering results in different forested landscapes. Compared with the existing methods, the main contributions of the proposed method are presented as follows:

- (1) A progressive plane detection method is proposed to characterize terrain. This method quantitatively evaluates the reliability of the planes with different sizes to represent local terrain and adopts the planes with optimal sizes according to evaluation results. Finally, terrain is characterized by multi-scale planes, that is, the local terrain with large slope variations is represented by small-scale planes and vice versa. This method provides a high-quality reference for ground point extraction on various terrains. More importantly, this method does not require setting the window size, improving its utility.
- (2) An improved surface-based filtering method is developed to extract ground points. The method uses the interior points of the multi-scale planes as ground seeds. Compared with the local minimum method, it can identify more ground seeds on various terrains (e.g., raised terrain) and is resistant to negative outliers. In addition, the neighbor ground points are extracted from multiple subspaces, ensuring the spatial uniform distribution of the selected neighbor ground points. These improvements increase the accuracy of ground point extraction.

## 2. Data and Method

The research framework consists of three parts, including data preparation, method design, and performance evaluation (Figure 1). First, the data with various terrain, vegetation, and point cloud features are prepared. Then, our method is designed, which can be divided into point extraction under forest canopy, progressive random sample consensus (RANSAC) plane detection, and ground point extraction. Point extraction under forest canopy aims to minimize the interference of non-ground points on the plane detection on the ground by eliminating the points with large height in a neighborhood. Based on the points under forest canopy, terrain is characterized based on multi-scale planes using progressive RANSAC plane detection. Ground points are extracted by selecting the points with small distance between them and the reference terrain characterized by planes. Finally, based on the prepared data, the performance of the proposed method is evaluated by adopting the accuracy metrics and comparing with classical filtering methods.

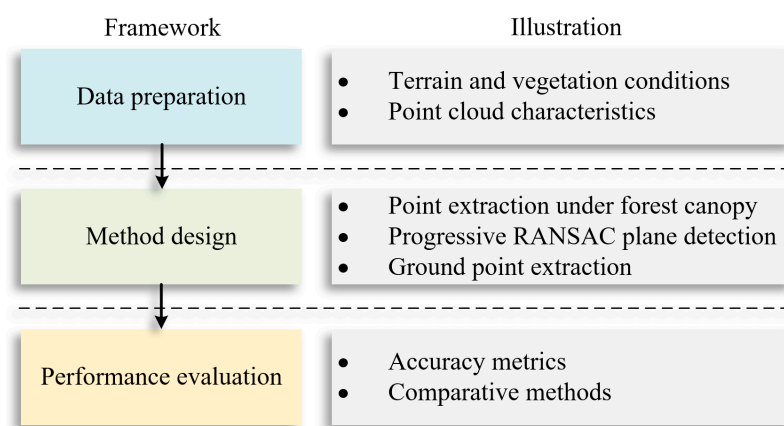


**Figure 1.** Research framework.

### 2.1. Data Description

We selected six  $300 \times 300$  m forested sites to evaluate the performance of the proposed method (Figure 2). LiDAR data for these sites is supplied by OpenTopography (California, America). The details of LiDAR data collection are summarized in Table 1. The data in Site 1 and Sites 2–6 were collected by Leica ALS50 (Leica, Gallen, Switzerland) and Optech GEMINI (Optech, Ontario, Canada) airborne laser terrain mapper, respectively. The collection was performed using flight altitudes of 600–900 m above the ground, scan frequencies of 40–83 Hz, scan angles of  $14\text{--}25^\circ$  from nadir, and adjacent swath overlaps of 50%–100%, generating average point densities of 2.16–21.74 points/m<sup>2</sup>.

**Table 1.** LiDAR data collection information for the six forested sites.

Site	Location	Collection Date	System	Flying Height (m)	Scan Frequency (Hz)	Scan Angle (°)	Overlap (%)	Mean Density (Points/m <sup>2</sup> )
1	Lake Tahoe, Sierra Nevada	August, 2010	Leica ALS50	900	83	14	100	21.74
2	North, Wasatch	July, 2008	Optech GEMINI ALTM	700	70	20	50	7.9
3	East, Modesto	August, 2010	Optech GEMINI ALTM	600	40	21	50	7.82
4	East, Ephrain	July, 2010	Optech GEMINI ALTM	600	40	21	50	6.73
5	Southeast, Butte	August, 2010	Optech GEMINI ALTM	600	40	21	50	8.1
6	West Reno	July, 2007	Optech GEMINI ALTM	700	40	25	50	2.16

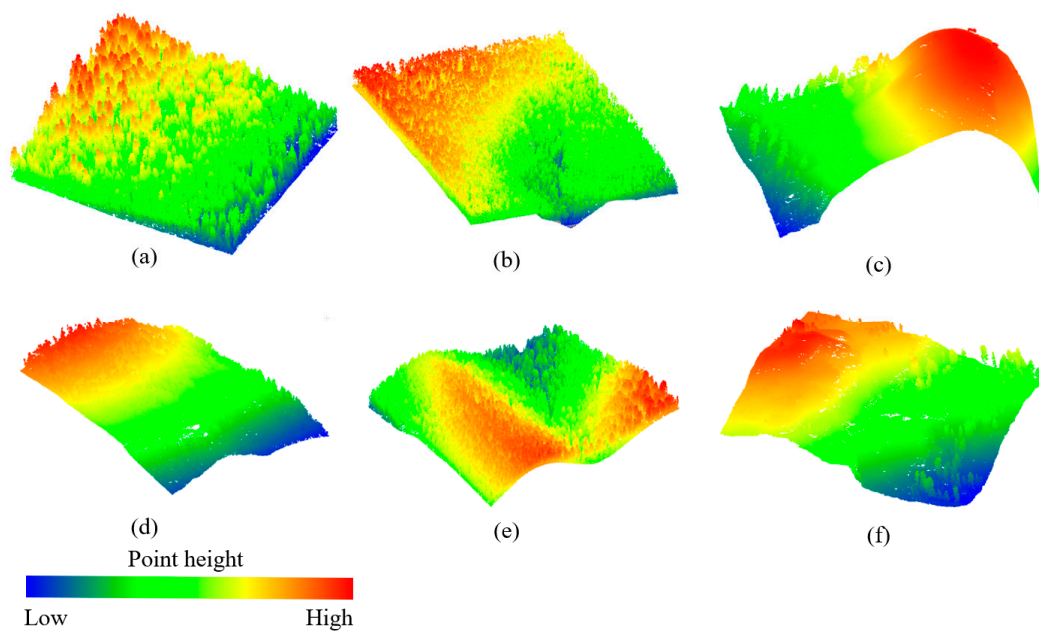


**Figure 2.** LiDAR point clouds of six forested sites: (a–f) Sites 1–6.

The statistics of terrain and vegetation conditions for six forested sites are shown in Figure 3. They were calculated based on reference ground and non-ground points, which were generated through human–computer interaction. The slope of local terrain in each plot was obtained by calculating the angles between horizontal planes and the local terrain surfaces that were constructed by fitting planes based on the neighbor ground points of each ground point. The 10 m pixel-level canopy cover was calculated based on canopy height models (CHMs). The 1 m resolution CHMs were generated from LiDAR point clouds and, then, the canopy cover of each 10 m grid cell was estimated by calculating the percentage of the pixels that are higher than 2 m [16,49]. Canopy height was counted from the pixels with height higher than 2 m in the 1 m resolution CHMs. The terrain slope, canopy cover, and canopy height maps of a sample site are given in Figure 4. These sites contain various terrain conditions (i.e., gentle slopes, steep slopes, hilltops, valleys, ridges, and break lines) with an average terrain slope of 18.3–37.11°. Furthermore, vegetation conditions vary widely with an average canopy cover of 7.27%–84.67% and canopy height of 7.83–23.6 m.

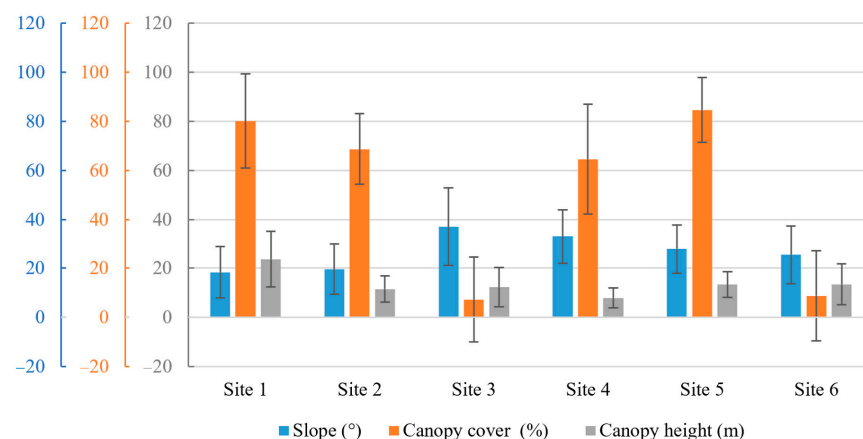


**Figure 3.** Statistics for the six forested sites.

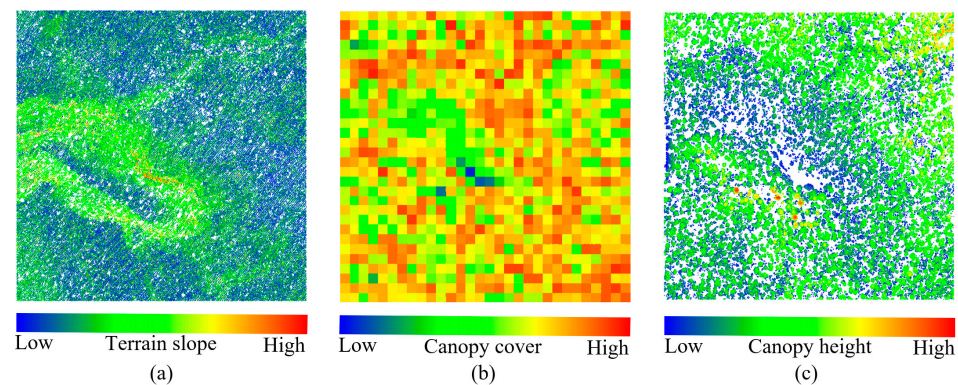


**Figure 4.** (a) Terrain slope, (b) canopy cover, and (c) canopy height maps for a sample site.

## 2.2. Overview of the Proposed Filtering Method

Irregular terrain can be characterized by multi-scale planes. The larger the slope variations of local terrain, the smaller the plane size should be (Figure 5). How to automatically detect the planes on the ground and determine optimal plane size are two core problems. Specifically, detecting planes on the ground of unfiltered LiDAR point clouds is difficult due to the negative influence of non-ground points. As a result, it is necessary to reduce non-ground points as much as possible before detecting planes and to adopt a plane detection method that is robust to noise (i.e., non-ground points). In terms of setting plane size, a small-scale plane can represent local terrain well, but the plane is often incorrectly detected in vegetation, since the number of ground points may not be dominant compared to vegetation points in a small region. In contrast, a large-scale plane tends to smooth local terrain with large slope variations, such as ridges and break lines. Thus, it is necessary to evaluate the reliability of the plane to represent local terrain and to determine optimal plane size based on evaluation results.

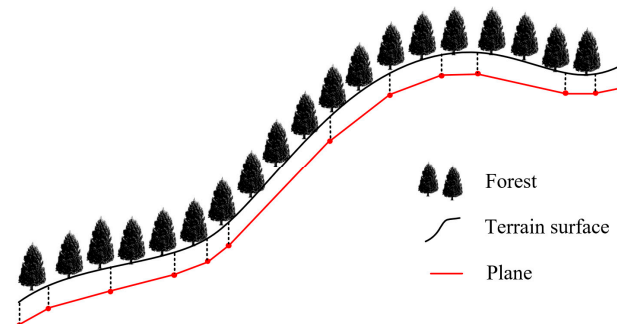


**Figure 5.** An illustration of irregular terrain characterized by multi-scale planes. The local terrain with larger slope variations is represented by the plane with smaller size.

To solve the two problems, a progressive plane detection method is proposed to characterize terrain. First, the points under forest canopy, which consist of ground and understory vegetation points, are extracted in unfiltered point clouds based on the feature that canopy points are higher than the points under forest canopy. Second, the points under forest canopy are divided into multiple regions and RANSAC plane detection method is adopted to detect planes in each region. It is because RANSAC has the advantage of being resistant to noise and, thus, has a greater potential to detect planes on the ground [50]. Next, the reliability of the plane representing local terrain is evaluated based on the maximum distance from the points under the detected plane to the plane. The smaller the distance is, the more reliable the plane is, and vice versa. If the reliability is low, the points in the region are further divided into multiple subregions with smaller size. The plane detection and reliability evaluation are iteratively performed, until no local terrain can be represented by planes. Finally, based on the terrain characterized by multi-scale planes, an improved

surface-based filtering method is developed to extract ground points. The method identifies ground seeds by selecting the interior points of the detected planes and, then, extracts ground points according to the distances of the points to the reference terrain, which is constructed with the neighbor ground points with spatially uniform distribution.

The proposed method is decomposed into three parts: point extraction under forest canopy, progressive RANSAC plane detection, and ground point extraction. In the following sections, the principle, implementation steps, and parameter settings in each part are described in detail, and the results of each part are verified by taking Site 2 as an example.

### 2.3. Point Extraction under Forest Canopy

The negative effects of non-ground points (mainly from forest canopy) require to be reduced as much as possible to detect planes on the ground. Otherwise, planes may be detected in non-ground objects even using anti-noise plane detection methods. The points under forest canopy are extracted according to the feature that these points are lower than canopy points in a local region. The points ( $P_{ufc}$ ) under the canopy are expressed as:

$$P_{ufc} = \{ p \mid h_p - h_0 < T_h \} \quad (1)$$

where  $p$  is an unclassified point;  $h_p$  is the height of  $p$ ;  $h_0$  is the height of the local minimum point; and  $T_h$  is the height threshold.

The implementation steps include regional division, seed identification under forest canopy, and point extraction under forest canopy. First, an unfiltered point cloud is gridded and a grid cell represents a local region. Then, the lowest points in each cell are identified as the seeds under forest canopy. Finally, the points under forest canopy are extracted based on the seeds under forest canopy cell by cell. In a cell, a point is identified as the point under forest canopy if the height difference between the point and the seed is less than a threshold.

This part includes two parameters, i.e., cell size and height difference. The cell size was set to 2 m, considering that the lowest point within 2 m is usually located under the forest canopy. The height difference was set to 5 m, since canopy points usually are 2–5 m above the ground according to the studies of canopy cover estimation [49,51]. To ensure that the ground points are completely preserved, the height difference was conservatively set to 5 m.

The points under forest canopy using the above procedure in a sample site (Site 2) are shown in Figure 6. Ground points are not only completely preserved but also most of forest canopy points (gray points) are accurately removed in gentle slopes and steep slopes (see enlarged figures A and B). Thus, the extracted points under forest canopy can provide an important basis for subsequent progressive RANSAC plane detection.

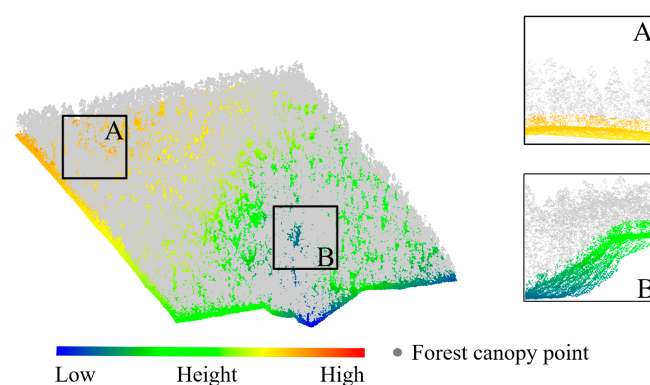


**Figure 6.** The results of point extraction under forest canopy in a sample site (Site 2). The proposed method can effectively extract the points under forest canopy in gentle slopes and steep slopes, as shown in the enlarged figures A and B.

#### 2.4. Progressive RANSAC Plane Detection

Based on the points under forest canopy, the RANSAC plane detection method is adopted to detect planes on the ground, since this method is robust to noise (including understory vegetation points and negative outliers). However, determining the optimal plane size is critical to describe the terrain in detail and accurately. To solve this problem, we propose a progressive RANSAC plane detection method with decreasing plane sizes. The method detects a plane in a local region and then evaluates the reliability of the plane to represent the terrain in the local region by calculating the maximum distance from points below the detected plane to the plane using Equation (2).

$$\frac{|ax_m + by_m + cz_m + d|}{\sqrt{a^2 + b^2 + c^2}} < T_d \quad (2)$$

where  $a$ ,  $b$ ,  $c$ , and  $d$  are the coefficients of the detected plane;  $(x_m, y_m, z_m)$  is the coordinate of the point  $p_m$  below the plane farthest from the plane; and  $T_d$  is the distance threshold. In the region with low reliability, the plane with smaller size is detected until the terrain cannot be characterized by a plane.

The implementation steps include regional division, plane detection, reliability evaluation of plane to represent local terrain, and regional subdivision. First, the points under forest canopy are gridded. The cell size of grid is the initial plane size for plane detection. Second, a plane is detected based on the points in a cell using RANSAC. The detected plane is preserved if the number of interior points for the plane is less than a threshold. Third, the maximum distance from the points under the detected plane to the plane is calculated. If the distance is lower than a division distance threshold, the ground in the cell can be represented with the current size plane. Fourth, the points in the cell with low reliability are further gridded with  $0.5 \times$  the cell size. Steps 2–4 are repeated until no planes can be detected.

The progressive RANSAC plane detection method has three parameters, including initial plane size, number of interior points, and division distance. These parameters were set to 10 m, 20 points, and 1 m empirically in this study.

The plane detection results in the sample site are shown in Figure 7. The local terrain is represented using planes of decreasing sizes as the slope variation increases. Specifically, gentle slopes, steep slopes, and discontinuous terrain are represented by large-, medium-, and small-scale planes (Figures 7a, 7b and 7c), respectively. This confirms that the proposed reliability evaluation method is effective. Thus, the terrain characterized by multi-scale planes can provide a complete and accurate reference for subsequent ground point extraction.

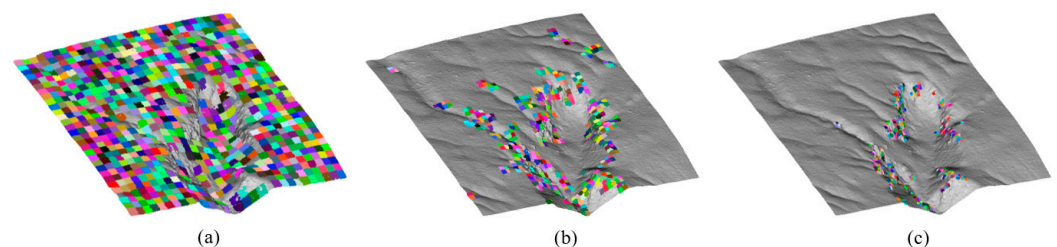


**Figure 7.** The results of progressive RANSAC plane detection in the sample site. (a) Gentle slopes, (b) steep slopes, and (c) discontinuous terrain are represented by large-, medium-, and small-scale planes, respectively. Colored square and gray surface indicate detected planes and true terrain, respectively.

#### 2.5. Ground Point Extraction

After the terrain is characterized by multi-scale planes, ground points are extracted using an improved surface-based filtering method. The main improvements of the method include two aspects. On the one hand, ground seeds are identified by selecting the points within buffers of detected planes, rather than the lowest points within sliding windows.

On the other hand, the reference terrain for ground point extraction is constructed using the neighbor ground points with spatially uniform distribution. Specifically, the method divides the two-dimensional local space into four subspaces with an unclassified point as center point (Figure 8) and, then, the ground points ( $P_n$ ) nearest to the center point in each subspace are extracted to construct the local reference terrain using Equation (3).

$$P_n = \begin{cases} p_1, & \text{if } x_p > x_o, y_p > y_o \text{ and } \arg \min \|\vec{op}\|_2 \\ p_2, & \text{if } x_p < x_o, y_p > y_o \text{ and } \arg \min \|\vec{op}\|_2 \\ p_3, & \text{if } x_p < x_o, y_p < y_o \text{ and } \arg \min \|\vec{op}\|_2 \\ p_4, & \text{if } x_p > x_o, y_p < y_o \text{ and } \arg \min \|\vec{op}\|_2 \end{cases} \quad (3)$$

where  $p_1, p_2, p_3$ , and  $p_4$  are the points selected in the four subspaces, respectively;  $(x_o, y_o)$  and  $(x_p, y_p)$  are the coordinates of the center point  $o$  and the neighbor point  $p$ , respectively; and  $\vec{op}$  is the vector between points  $o$  and  $p$ .

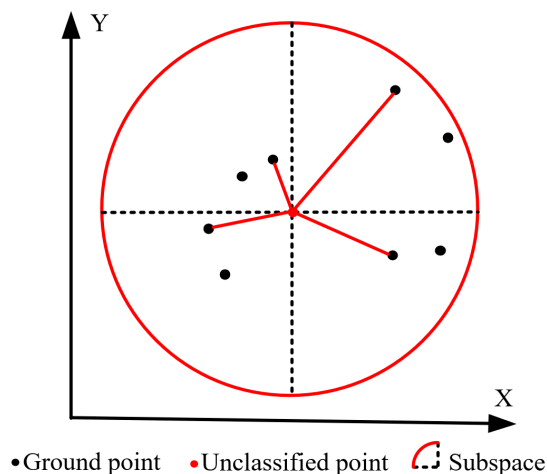


**Figure 8.** Schematic diagram of the identification for evenly distributed neighbor ground points.

The implementation steps include point cloud attribute initialization, ground seed identification, and ground point extraction. First, the attributes of all points in the point cloud are marked as unclassified points. Second, unclassified points are regarded as ground seeds if the distances between the points and the detected planes are less than a buffer difference threshold. The attributes of identified ground seeds are modified to ground points. Third, the neighbor ground points of an unclassified point are searched from multiple subspaces. The local reference terrain is constructed based on the searched ground points using the least-squares plane fitting method. The unclassified point is marked as ground point if the distance between the point and the local reference terrain is less than a classification distance threshold. Step 3 is repeated until no points are classified as ground points.

The part includes two parameters, i.e., buffer difference and classification distance. They were set to 0.5 m and 1.5 m empirically in this study.

The results of ground seed identification and ground point extraction in the sample are shown in Figures 9 and 10, respectively. Compared with the local minimum method (Figure 9a), the proposed method can identify more ground points on various terrain details (Figure 9b), which provides a more detailed reference for ground point extraction. In addition, the proposed method obtains more accurate ground filtering results than the traditional  $k$ -nearest neighbor method in regions with uneven ground points (see enlarged figures A and B in Figure 10).

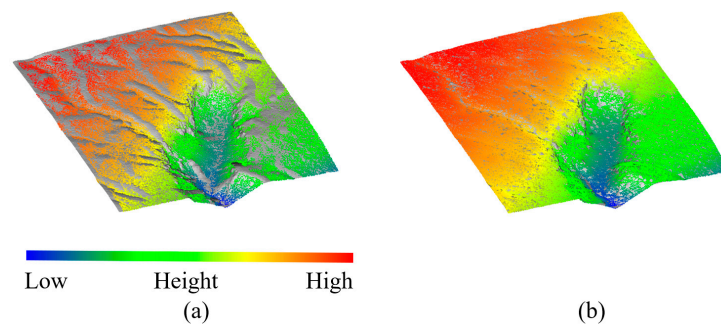
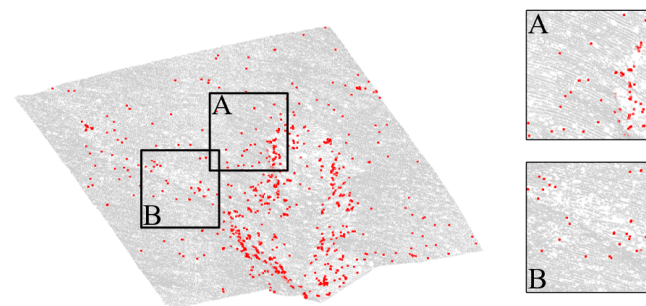


**Figure 9.** Ground seeds identified by (a) the local minimum method and (b) the proposed method. Gray surface indicates true terrain.



- True ground point
- Ground point that can only be identified by ours

**Figure 10.** The ground points that can be identified only by the proposed method compared to the traditional  $k$ -nearest neighbor method. The proposed method obtains more accurate ground filtering results in the regions with uneven ground points, as shown in the enlarged figures A and B.

## 2.6. Experimental Setup

The experiments were carried out on a laptop computer with 40 GB RAM and an AMD Ryzen 7 5800 H with Radeon Graphics @ 3.20 GHz. The details of the experiments, including accuracy metrics and comparative methods, are given in this section.

### 2.6.1. Accuracy Metrics

We quantitatively evaluated the performance of ground filtering methods using type I error, type II error, and total error for all sites [52]. Type I error indicates the proportion of ground points being misclassified into non-ground points (Equation (4)). Type II error represents the proportion of opposite condition (Equation (5)). Total error is the proportion of all misclassified points (Equation (6)).

$$\text{Type I} = \frac{a}{c} \quad (4)$$

$$\text{Type II} = \frac{b}{d} \quad (5)$$

$$\text{Total} = \frac{a + b}{c + d} \quad (6)$$

where  $a$  is the number of ground points misclassified as non-ground points,  $b$  is the number of non-ground points misclassified as ground points, and  $c$  and  $d$  are the number of reference ground points and non-ground points.

### 2.6.2. Comparative Methods

The proposed method was compared with four well-known filtering methods, including maximum slope filtering (MSF) [20], progressive morphology filtering (PMF) [26], cloth simulation filtering (CSF) [19], and progressive triangular irregular network densification filtering (PTDF) methods [35]. As described in Section 1, MSF and PMF belong to the slope-based and mathematical morphology-based methods, respectively, while CSF and PTDF belong to the surface-based methods. MSF was implemented using the C++ programming language. PMF was implemented using the C++ programming language and the PCL library [53]. CSF was implemented using CloudCompare software v2.11.3 (Daniel Girardeau, Grenoble, France) [54]. PTDF was implemented using Terrasolid software V8i (Terrasolid, Espoo, Finland) [55]. Table 2 lists the parameter settings of the comparative methods. These parameters were set by visually determining whether most ground points and non-ground points were accurately distinguished. Specifically, the filtered point cloud was segmented into multiple strips with the width of 50 m, because ground filtering results can be better checked in cross-section view. We observed the results from different views in CloudCompare software v2.11.3 (Daniel Girardeau, Grenoble, France) and selected the parameter settings corresponding to the optimal results.

**Table 2.** Parameter settings of the comparative methods. MSF, PMF, CSF, and PTDF represent the four comparative methods, i.e., maximum slope filtering, progressive morphology filtering, cloth simulation filtering, and progressive triangular irregular network densification filtering methods.

Method	Parameter			
MSF	Cell size: 1 m	Window size: 10 m	Slope: 15°	Maximum height: 3 m
PMF	Window size: 10 m	Slope: 15°	Initial height: 0.5 m	Maximum height: 3 m
CSF	Rigidity: 3	Cloth resolution: 0.3 m	Max iterations: 500	Classification threshold: 0.5 m
PTDF	Window size: 10 m	Terrain angle: 88°	Iteration angle: 15 °	Iteration distance: 1.5 m

### 3. Results

The accuracy comparison of the proposed method (i.e., PPDF) and the comparative methods (i.e., MSF, PMF, CSF, and PTDF) are given in Figure 11. PPDF had the lowest average total error of 3.42% and standard deviation of 2.45% across all sites, which include various terrain (e.g., terrain slope and height) and vegetation conditions (e.g., canopy cover and height). PPDF also achieved high accuracy with less than 5% total error even in sites (e.g., Sites 2 and 6) containing dense vegetation and various discontinuous terrain. The smallest type I errors were achieved by the proposed method in five out of six sites, and the total error in the remaining sample (i.e., Site 1) was rather close to the optimal result, with a difference of 0.34%. In terms of type II errors, the proposed method obtained optimal or near-optimal results in most sites.

The digital terrain models (DTMs) constructed by the proposed method were highly similar to the reference DTMs in all forested sites. The proposed method completely preserved various terrain features, including the gentle slopes in Site 1 (Figure 12a), valleys in Site 2 (Figure 12b), steep slopes in Site 3 (Figure 12c), hilltops in Site 4 (Figure 12d), ridges in Site 5 (Figure 12e), and break lines in Site 6 (Figure 12f). Meanwhile, vegetation points with different cover and height values were effectively filtered out.

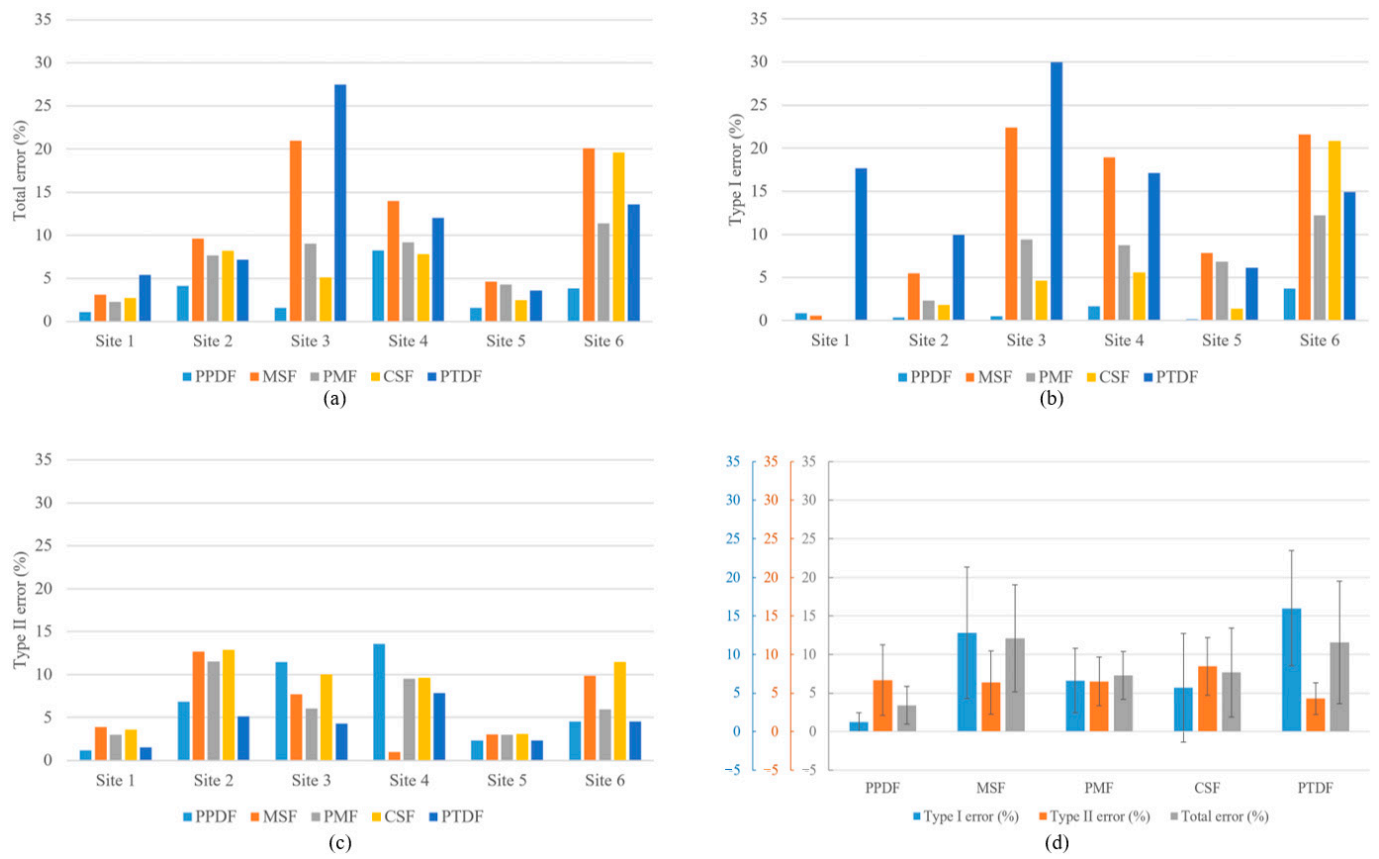


**Figure 11.** Accuracy comparison of the proposed method and the comparative methods: (a) total error, (b) type I error, (c) type II error, and (d) average and standard deviation values of the three errors. MSF, PMF, CSF, and PTFD represent the four comparative methods, i.e., maximum slope filtering, progressive morphology filtering, cloth simulation filtering, and progressive triangular irregular network densification filtering methods.

Figures 13 and 14 show the DTMs of the proposed and well-known ground filtering methods for two representative sites (Sites 2 and 6), which are characterized by high canopy cover and various discontinuous terrain, respectively. In Site 2, the proposed method generated DTM that are closer to the reference result. In comparison, MSF failed to preserve highly steep slopes and ridges (see ellipses A and B in Figure 13) and accurately filtered out vegetation points (see ellipse C in Figure 13). PMF often smoothed ridges (see ellipse C in Figure 13). CSF tended to misclassify vegetation points as ground points (see ellipse B in Figure 13). PTFD often smoothed highly steep slopes (see ellipse A in Figure 13). In Site 6, various morphological break lines were preserved more realistically by the proposed method compared to other methods, as shown in ellipses A, B, and C in Figure 14.

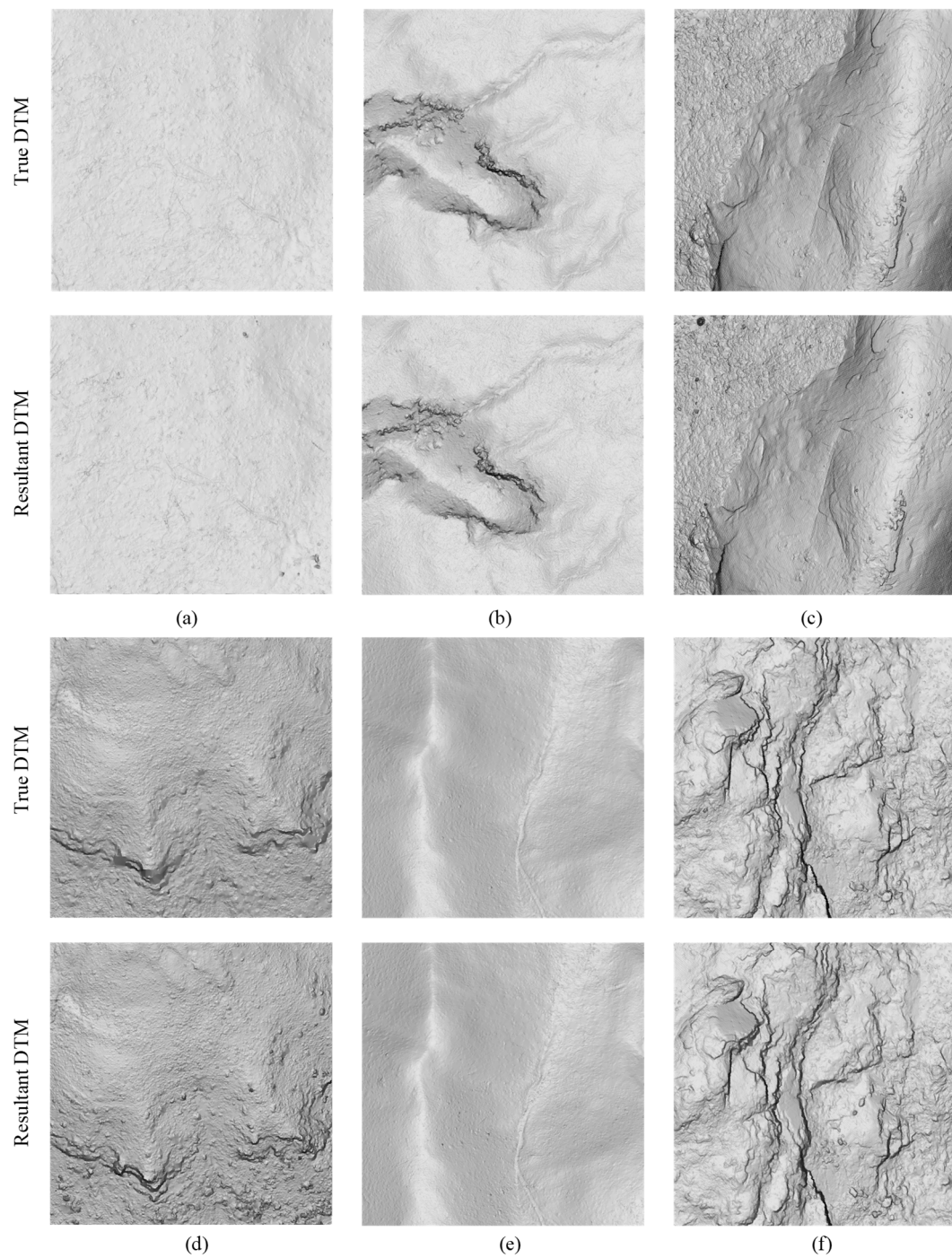


**Figure 12.** DTMs of the proposed method in all sites: (a–f) Sites 1–6.

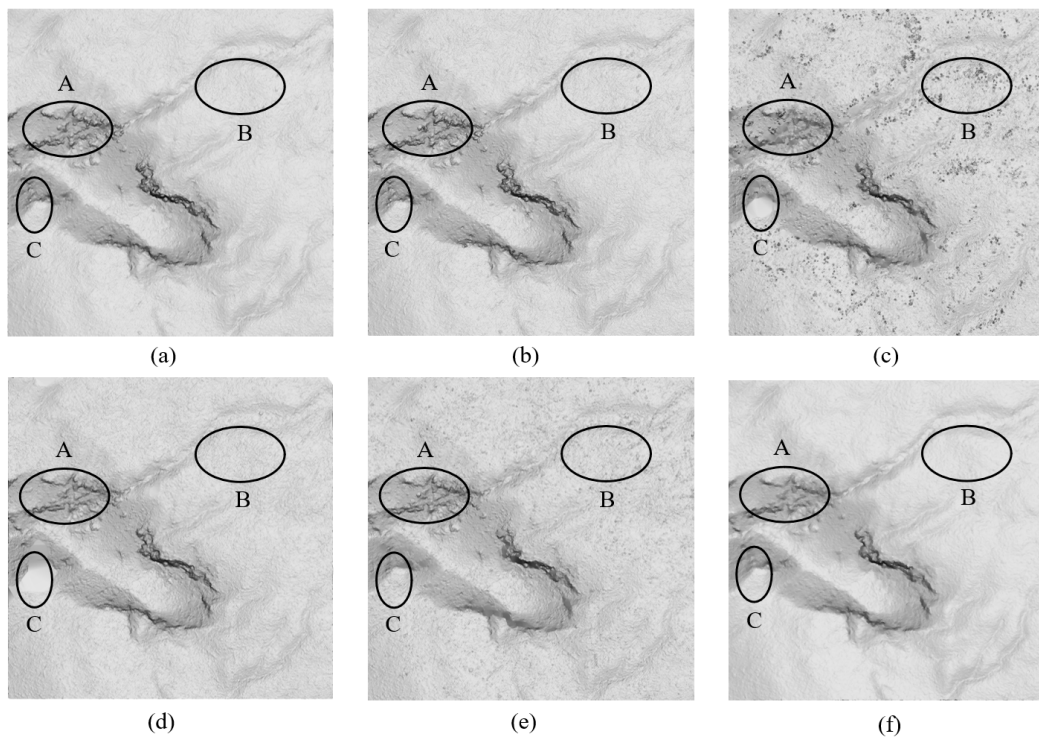


**Figure 13.** DTMs of (a) reference, (b) PPDF, (c) MSF, (d) PMF, (e) CSF, and (f) PTDF in Site 2. MSF, PMF, CSF, and PTDF represent the four comparative methods, i.e., maximum slope filtering, progressive morphology filtering, cloth simulation filtering, and progressive triangular irregular network densification filtering methods.

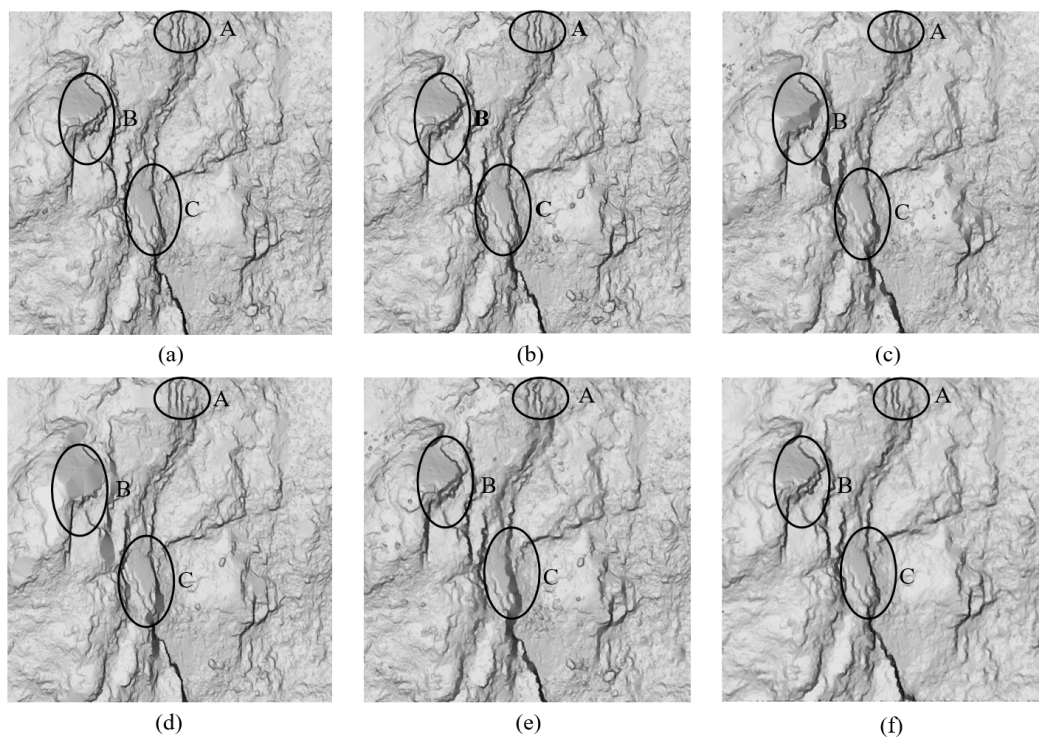


**Figure 14.** DTMs of (a) reference, (b) PPDF, (c) MSF, (d) PMF, (e) CSF and (f) PTDF in Site 6. MSF, PMF, CSF and PTDF represent the four comparative methods, i.e., maximum slope filtering, progressive morphology filtering, cloth simulation filtering, and progressive triangular irregular network densification filtering methods.

The computational efficiency comparison between the proposed method and well-known methods is given in Figure 15. The proposed method was comparable to PMF and CSF, and significantly higher than PMF. In addition, the computational efficiency of the proposed method was negatively related to the point density. Site 1, Sites 2–5, and Site 6 had high, medium, and low point densities and exhibited the same trend in runtime. Note that the computational efficiency of PTDF was not evaluated, since Terrsolid software V8i (Terrsolid, Espoo, Finland) cannot provide runtime information.

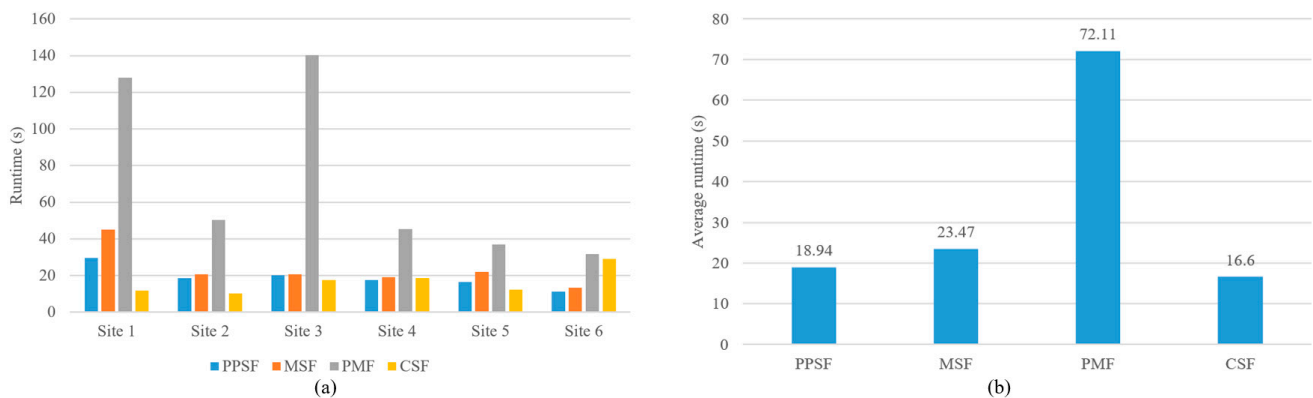


**Figure 15.** Runtime comparison between the proposed and well-known ground filtering methods in terms of (a) each forested site and (b) their average values. MSF, PMF, CSF, and PTDF represent the four comparative methods, i.e., maximum slope filtering, progressive morphology filtering, cloth simulation filtering, and progressive triangular irregular network densification filtering methods.

## 4. Discussion

### 4.1. Performance Analysis

Compared with other methods, PPSF was more accurate and more robust even in the landscapes containing dense vegetation and complex terrain, with the smallest average total error and standard deviation (Figure 11). This is attributed to the contributions described in Section 1. To test the performance of the proposed method with and without each contribution, we performed two tests in all sites. The accuracy comparison between the proposed method with and without the two contributions is given in Figure 16. Results showed that both contributions helped to improve ground filtering accuracy in all sites. For the average total errors of the proposed method with both contributions, only the first contribution and the second contribution were 3.42%, 3.75%, and 9.12%, respectively. In comparison, the contribution of the progressive plane detection method was greater especially in the sites containing the terrain with large slope variations, e.g., Site 6.

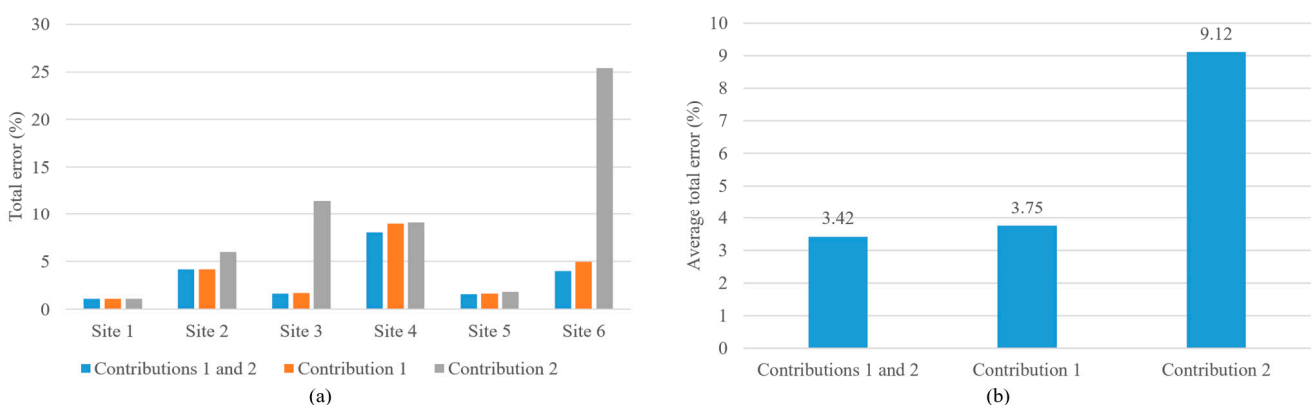


**Figure 16.** Accuracy comparison of the proposed method with and without each contribution in terms of (a) each forested site and (b) their average values.

PPDF had obviously higher a ground filtering accuracy than MSF (Figure 11). The possible reasons include two aspects. On the one hand, MSF fails to obtain ground seeds on raised terrain and negative outliers may also be misjudged as ground seeds. On the other hand, MSF judges the attributes of unclassified points only based on the nearest neighbor ground points. In contrast, PPDF can obtain more complete ground seeds on various terrains based on the terrain characterized by multi-scale planes. The misjudgment of negative outliers as ground seeds can also be avoided due to the introduction of the feature that the local terrain is flat. Additionally, ground points are extracted based on the reference terrain which uses more contexts. As a result, the proposed method outperforms MSF. Although PMF can obtain more ground seeds than MSF, it still cannot select enough ground seeds on raised terrain, causing the terrain to be smoothed (Figures 13d and 14d). Nevertheless, PPDF overcomes this limitation by identifying ground seeds based on the feature that the local terrain is flat, rather than the local minimum (Figures 13b and 14b). CSF often produces filtering errors probably because it only extracts ground points based on the nearest neighbor ground points (Figure 13e). However, PPDF reduces these errors by using a reference terrain that contains more context. PTDF tends to ignore terrain details, especially in the sites with steep slopes and break lines (Figures 13f and 14f). Although PTDF cannot obtain sufficient ground seeds on the terrain, PTDF extracts ground points through iterative upward densification, that is, ground points are extracted from points above the reference terrain in each iteration [16,39]. However, PPDF identifies ground points by iteratively upward and downward densification, thus, better preserving the terrain's details. Overall, PPDF has advantages over other methods in terms of accuracy and reliability.

#### 4.2. Parameter Sensitivity Analysis

The sensitivity of PPDF to key parameters was evaluated, considering that the parameter settings in different landscapes are a core factor affecting the ease of use for the method. We iteratively executed the proposed method by replacing one parameter with a certain interval while keeping other parameters at default settings. The influence of each parameter on filtering the results is given in Figure 17. The effect of initial plane size on the total error was limited even using a particularly large plane size (Figure 17a), because the optimal plane size can be automatically and accurately determined by evaluating the reliability of the plane to represent the local terrain. The number of interior points had insignificant influences on filtering the results (Figure 17b). There was no obvious accuracy difference with the change in the division distance threshold (Figure 17c). The effect of the classification distance on filtering the results was small in a large interval (Figure 17d), probably because a more detailed reference terrain weakens the dependence of surface-based filtering methods on the classification of the distance threshold [14,16,47]. In general, these results suggested that the proposed method was insensitive to the settings of the initial plane size, the number of interior points, the division distance, and the classification distance, and these parameters can be set to fixed values.

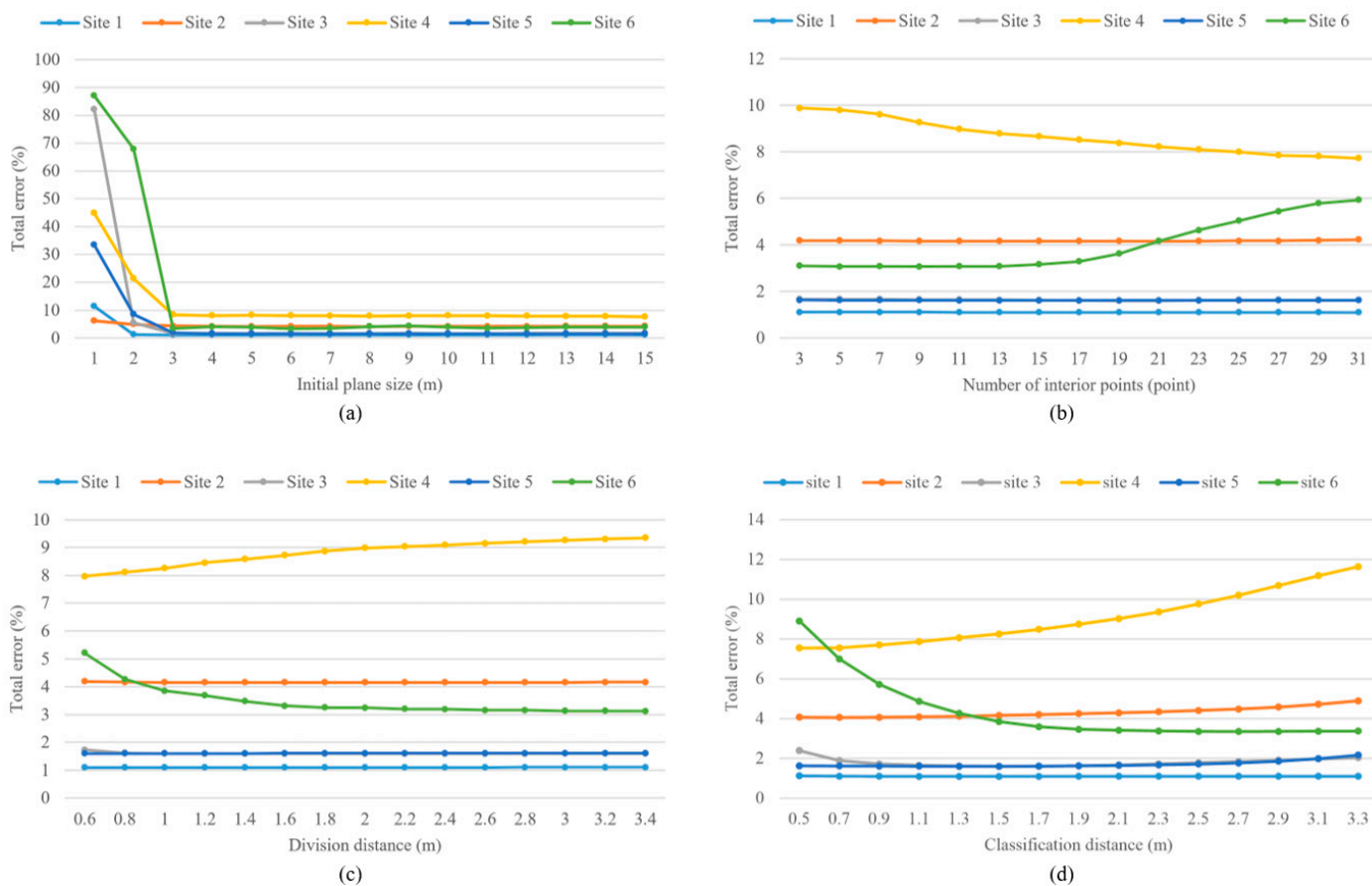


**Figure 17.** The sensitivity of the proposed method to the settings of (a) initial plane size, (b) number of interior points, (c) division distance, and (d) classification distance. Experiments were performed in each site. Only one parameter was adjusted in each execution, while other parameters were kept at default settings.

### 5. Conclusions

To improve the effectiveness and ease of use of ground filtering in forested landscapes containing dense vegetation and complex terrain, a progressive plane detection filtering method for airborne LiDAR point clouds is proposed in this study. The novelty of the proposed method lies within its use of progressive plane detection to identify ground seeds as completely as possible on various terrains and the identification of evenly distributed neighbor ground points to construct a reference terrain to increase the accuracy of ground point extraction in the regions with uneven ground points. We demonstrated the effectiveness of the proposed method by quantitatively and qualitatively comparing four classic filtering methods, which belong to different types of filtering methods that have been published. Meanwhile, the ease of use of the proposed method was verified by testing the sensitivity of the proposed method to the parameters. There are two major conclusions.

- (1) The proposed method can improve the effectiveness of ground filtering in the forested landscapes. It achieved the smallest average total error and standard deviation compared to other methods and the preservation of terrain details was greatly improved especially in regions with large terrain slope variations (e.g., steep slopes, break lines, and ridges).
- (2) The proposed method has the advantage of ease of use. It was insensitive to parameters. Therefore, these parameters can be set as fixed values, which makes it easier for the users with insufficient experience to execute ground filtering in their own applications.

**Author Contributions:** Conceptualization, S.C.; data curation, S.C.; formal analysis, S.C. and S.Y.; funding acquisition, X.L.; investigation, S.C.; methodology, S.C. and X.L.; project administration, S.C. and X.L.; resources, S.C. and X.L.; software, S.C.; supervision, S.C. and X.L.; validation, S.C. and S.Y.; visualization, S.C.; writing—original draft, S.C.; writing—review and editing, S.C., X.L. and S.Y. All authors have read and agreed to the published version of the manuscript.

**Funding:** This research was funded by the Natural Science Fund of China, grant number 32171789, 32211530031; Wuhan University, grant number WHUZZJJ202220; Open Fund of Key Laboratory of Mine Environmental Monitoring and Improving around Poyang Lake, Ministry of Natural Resources, grant number MEMI-2021-2022-03; International S&T Cooperation Program of Hubei Province, grant number 2022EHB048; National Key R&D Program of China, grant number 2022YFB3903800; Open Fund of Key Research Base of Philosophy and Social Science of Higher Education in Guangdong Province - Local Government Development Research Institute of Shantou University, grant number 07422002.

**Data Availability Statement:** The authors do not have permission to share data.

**Conflicts of Interest:** The authors declare no conflict of interest.

## References

- Drake, J.B.; Dubayah, R.O.; Clark, D.B.; Knox, R.G.; Blair, J.B.; Hofton, M.A.; Chazdon, R.L.; Weishampel, J.F.; Prince, S. Estimation of tropical forest structural characteristics using large-footprint lidar. *Remote Sens. Environ.* **2002**, *79*, 305–319. [\[CrossRef\]](#)
- Brandtberg, T. Classifying individual tree species under leaf-off and leaf-on conditions using airborne lidar. *ISPRS J. Photogramm. Remote Sens.* **2007**, *61*, 325–340. [\[CrossRef\]](#)
- Popescu, S.C. Estimating biomass of individual pine trees using airborne lidar. *Biomass Bioenergy* **2007**, *31*, 646–655. [\[CrossRef\]](#)
- Hyyppä, J.; Yu, X.; Hyyppä, H.; Vastaranta, M.; Holopainen, M.; Kukko, A.; Kaartinen, H.; Jaakkola, A.; Vaaja, M.; Koskinen, J.; et al. Advances in Forest Inventory Using Airborne Laser Scanning. *Remote Sens.* **2012**, *4*, 1190–1207. [\[CrossRef\]](#)
- Hyyppä, J.; Hyyppä, H.; Leckie, D.; Gougeon, F.; Yu, X.; Maltamo, M. Review of methods of small-footprint airborne laser scanning for extracting forest inventory data in boreal forests. *Int. J. Remote Sens.* **2008**, *29*, 1339–1366. [\[CrossRef\]](#)
- Wulder, M.A.; White, J.C.; Nelson, R.F.; Næsset, E.; Ørka, H.O.; Coops, N.C.; Hilker, T.; Bater, C.W.; Gobakken, T. Lidar Sampling for Large-Area Forest Characterization: A Review. *Remote Sens. Environ.* **2012**, *121*, 196–209. [\[CrossRef\]](#)
- Ferraz, A.; Bretar, F.; Jacquemoud, S.; Gonçalves, G.; Pereira, L.; Tomé, M.; Soares, P. 3-D mapping of a multi-layered Mediterranean forest using ALS data. *Remote Sens. Environ.* **2012**, *121*, 210–223. [\[CrossRef\]](#)
- Shi, Y.; Wang, T.; Skidmore, A.K.; Heurich, M. Important LiDAR metrics for discriminating forest tree species in Central Europe. *ISPRS J. Photogramm. Remote Sens.* **2018**, *137*, 163–174. [\[CrossRef\]](#)
- Mielcarek, M.; Stereńczak, K.; Khosravipour, A. Testing and evaluating different LiDAR-derived canopy height model generation methods for tree height estimation. *Int. J. Appl. Earth Obs. Geoinf.* **2018**, *71*, 132–143. [\[CrossRef\]](#)
- Dai, W.; Guan, Q.; Cai, S.; Liu, R.; Chen, R.; Liu, Q.; Chen, C.; Dong, Z. A Comparison of the Performances of Unmanned-Aerial-Vehicle (UAV) and Terrestrial Laser Scanning for Forest Plot Canopy Cover Estimation in *Pinus massoniana* Forests. *Remote Sens.* **2022**, *14*, 1188. [\[CrossRef\]](#)
- Hartling, S.; Sagan, V.; Sidike, P.; Maimaitijiang, M.; Carron, J. Urban Tree Species Classification Using a WorldView-2/3 and LiDAR Data Fusion Approach and Deep Learning. *Sensors* **2019**, *19*, 1284. [\[CrossRef\]](#)
- Liang, X.; Wang, Y.; Pyörälä, J.; Lehtomäki, M.; Yu, X.; Kaartinen, H.; Kukko, A.; Honkavaara, E.; Issaoui, A.E.I.; Nevalainen, O.; et al. Forest in situ observations using unmanned aerial vehicle as an alternative of terrestrial measurements. *For. Ecosyst.* **2019**, *6*, 20. [\[CrossRef\]](#)
- Liang, X.; Kukko, A.; Balenovic, I.; Saarinen, N.; Junttila, S.; Kankare, V.; Holopainen, M.; Mokros, M.; Surovy, P.; Kaartinen, H.; et al. Close-Range Remote Sensing of Forests: The state of the art, challenges, and opportunities for systems and data acquisitions. *IEEE Geosci. Remote Sens. Mag.* **2022**, *10*, 32–71. [\[CrossRef\]](#)
- Chen, C.; Wang, M.; Chang, B.; Li, Y. Multi-Level Interpolation-Based Filter for Airborne LiDAR Point Clouds in Forested Areas. *IEEE Access* **2020**, *8*, 41000–41012. [\[CrossRef\]](#)
- Hui, Z.; Jin, S.; Xia, Y.; Nie, Y.; Xie, X.; Li, N. A mean shift segmentation morphological filter for airborne LiDAR DTM extraction under forest canopy. *Opt. Laser Technol.* **2021**, *136*, 106728. [\[CrossRef\]](#)
- Zhao, X.; Guo, Q.; Su, Y.; Xue, B. Improved progressive TIN densification filtering algorithm for airborne LiDAR data in forested areas. *ISPRS J. Photogramm. Remote Sens.* **2016**, *117*, 79–91. [\[CrossRef\]](#)
- Véga, C.; Durrieu, S.; Morel, J.; Allouis, T. A sequential iterative dual-filter for Lidar terrain modeling optimized for complex forested environments. *Comput. Geosci.* **2012**, *44*, 31–41. [\[CrossRef\]](#)
- Bigdeli, B.; Amirkolae, H.A.; Pahlavani, P. DTM extraction under forest canopy using LiDAR data and a modified invasive weed optimization algorithm. *Remote Sens. Environ.* **2018**, *216*, 289–300. [\[CrossRef\]](#)
- Zhang, W.; Qi, J.; Wan, P.; Wang, H.; Xie, D.; Wang, X.; Yan, G. An Easy-to-Use Airborne LiDAR Data Filtering Method Based on Cloth Simulation. *Remote Sens.* **2016**, *8*, 501. [\[CrossRef\]](#)

20. Vosselman, G. Slope Based Filtering of Laser Altimetry Data. *Int. Arch. Photogramm. Remote Sens.* **2000**, *33*, 935–942.
21. Meng, X.; Wang, L.; Silván-Cárdenas, J.L.; Currit, N. A multi-directional ground filtering algorithm for airborne LIDAR. *ISPRS J. Photogramm. Remote Sens.* **2009**, *64*, 117–124. [[CrossRef](#)]
22. Susaki, J. Adaptive Slope Filtering of Airborne LiDAR Data in Urban Areas for Digital Terrain Model (DTM) Generation. *Remote Sens.* **2012**, *4*, 1804–1819. [[CrossRef](#)]
23. Shan, J.; Aparajithan, S. Urban DEM Generation from Raw Lidar Data. *Photogramm. Eng. Remote Sens.* **2005**, *71*, 217–226. [[CrossRef](#)]
24. Chen, Z.; Gao, B.; Devereux, B. State-of-the-Art: DTM Generation Using Airborne LIDAR Data. *Sensors* **2017**, *17*, 150. [[CrossRef](#)]
25. Wan, P.; Zhang, W.; Skidmore, A.K.; Qi, J.; Jin, X.; Yan, G.; Wang, T. A simple terrain relief index for tuning slope-related parameters of LiDAR ground filtering algorithms. *ISPRS J. Photogramm. Remote Sens.* **2018**, *143*, 181–190. [[CrossRef](#)]
26. Zhang, K.; Chen, S.-C.; Whitman, D.; Shyu, M.-L.; Yan, J.; Zhang, C. A progressive morphological filter for removing nonground measurements from airborne LIDAR data. *IEEE Trans. Geosci. Remote Sens.* **2003**, *41*, 872–882. [[CrossRef](#)]
27. Pingel, T.J.; Clarke, K.C.; McBride, W.A. An improved simple morphological filter for the terrain classification of airborne LIDAR data. *ISPRS J. Photogramm. Remote Sens.* **2013**, *77*, 21–30. [[CrossRef](#)]
28. Li, Y.; Yong, B.; Wu, H.; An, R.; Xu, H. An Improved Top-Hat Filter with Sloped Brim for Extracting Ground Points from Airborne Lidar Point Clouds. *Remote Sens.* **2014**, *6*, 12885–12908. [[CrossRef](#)]
29. Mongus, D.; Lukač, N.; Žalik, B. Ground and building extraction from LiDAR data based on differential morphological profiles and locally fitted surfaces. *ISPRS J. Photogramm. Remote Sens.* **2014**, *93*, 145–156. [[CrossRef](#)]
30. Yang, B.; Huang, R.; Dong, Z.; Zang, Y.; Li, J. Two-step adaptive extraction method for ground points and breaklines from lidar point clouds. *ISPRS J. Photogramm. Remote Sens.* **2016**, *119*, 373–389. [[CrossRef](#)]
31. Chen, Q.; Gong, P.; Baldocchi, D.; Xie, G. Filtering Airborne Laser Scanning Data with Morphological Methods. *Photogramm. Eng. Remote Sens.* **2007**, *73*, 175–185. [[CrossRef](#)]
32. Chen, D.; Zhang, L.; Wang, Z.; Deng, H. A mathematical morphology-based multi-level filter of LiDAR data for generating DTMs. *Sci. China Inf. Sci.* **2012**, *56*, 1–14. [[CrossRef](#)]
33. Tan, Y.; Wang, S.; Xu, B.; Zhang, J. An improved progressive morphological filter for UAV-based photogrammetric point clouds in river bank monitoring. *ISPRS J. Photogramm. Remote Sens.* **2018**, *146*, 421–429. [[CrossRef](#)]
34. Liang, X.; Zhang, J.; Li, H. An Adaptive Morphological Filter for LIDAR Data Filtering in Urban Area. *J. Remote Sens.* **2007**, *2*, 276–281. [[CrossRef](#)]
35. Axelsson, P. DEM Generation from Laser Scanner Data Using Adaptive TIN Models. *Int. Arch. Photogramm. Remote Sens.* **2000**, *33*, 111–118.
36. Zhang, J.; Lin, X. Filtering airborne LiDAR data by embedding smoothness-constrained segmentation in progressive TIN densification. *ISPRS J. Photogramm. Remote Sens.* **2013**, *81*, 44–59. [[CrossRef](#)]
37. Hu, H.; Ding, Y.; Zhu, Q.; Wu, B.; Lin, H.; Du, Z.; Zhang, Y.; Zhang, Y. An adaptive surface filter for airborne laser scanning point clouds by means of regularization and bending energy. *ISPRS J. Photogramm. Remote Sens.* **2014**, *92*, 98–111. [[CrossRef](#)]
38. Evans, J.S.; Hudak, A.T. A Multiscale Curvature Algorithm for Classifying Discrete Return LiDAR in Forested Environments. *IEEE Trans. Geosci. Remote Sens.* **2007**, *45*, 1029–1038. [[CrossRef](#)]
39. Nie, S.; Wang, C.; Dong, P.; Xi, X.; Luo, S.; Qin, H. A revised progressive TIN densification for filtering airborne LiDAR data. *Measurement* **2017**, *104*, 70–77. [[CrossRef](#)]
40. Chen, C.; Chang, B.; Li, Y.; Shi, B. Filtering airborne LiDAR point clouds based on a scale-irrelevant and terrain-adaptive approach. *Measurement* **2021**, *171*, 108756. [[CrossRef](#)]
41. Chen, C.; Li, Y.; Li, W.; Dai, H. A multiresolution hierarchical classification algorithm for filtering airborne LiDAR data. *ISPRS J. Photogramm. Remote Sens.* **2013**, *82*, 1–9. [[CrossRef](#)]
42. Meng, X.; Lin, Y.; Yan, L.; Gao, X.; Yao, Y.; Wang, C.; Luo, S. Airborne LiDAR Point Cloud Filtering by a Multilevel Adaptive Filter Based on Morphological Reconstruction and Thin Plate Spline Interpolation. *Electronics* **2019**, *8*, 1153. [[CrossRef](#)]
43. Meng, X.; Currit, N.; Zhao, K. Ground Filtering Algorithms for Airborne LiDAR Data: A Review of Critical Issues. *Remote Sens.* **2010**, *2*, 833–860. [[CrossRef](#)]
44. Chen, C.; Guo, J.; Wu, H.; Li, Y.; Shi, B. Performance Comparison of Filtering Algorithms for High-Density Airborne LiDAR Point Clouds over Complex LandScapes. *Remote Sens.* **2021**, *13*, 2663. [[CrossRef](#)]
45. Hui, Z.; Wang, L.; Ziggah, Y.Y.; Cai, S.; Xia, Y. Automatic morphological filtering algorithm for airborne lidar data in urban areas. *Appl. Opt.* **2019**, *58*, 1164–1173. [[CrossRef](#)]
46. Wei, L.; Yang, B.; Jiang, J.; Cao, G.; Wu, M. Vegetation filtering algorithm for UAV-borne lidar point clouds: A case study in the middle-lower Yangtze River riparian zone. *Int. J. Remote Sens.* **2016**, *38*, 2991–3002. [[CrossRef](#)]
47. Cai, S.; Zhang, W.; Liang, X.; Wan, P.; Qi, J.; Yu, S.; Yan, G.; Shao, J. Filtering Airborne LiDAR Data Through Complementary Cloth Simulation and Progressive TIN Densification Filters. *Remote Sens.* **2019**, *11*, 1037. [[CrossRef](#)]
48. Hui, Z.; Hu, Y.; Yevenyo, Y.Z.; Yu, X. An Improved Morphological Algorithm for Filtering Airborne LiDAR Point Cloud Based on Multi-Level Kriging Interpolation. *Remote Sens.* **2016**, *8*, 35. [[CrossRef](#)]
49. Cai, S.; Zhang, W.; Jin, S.; Shao, J.; Li, L.; Yu, S.; Yan, G. Improving the estimation of canopy cover from UAV-LiDAR data using a pit-free CHM-based method. *Int. J. Digit. Earth* **2021**, *14*, 1477–1492. [[CrossRef](#)]

50. Daghigh, H.; Tannant, D.D.; Daghigh, V.; Lichti, D.D.; Lindenbergh, R. A critical review of discontinuity plane extraction from 3D point cloud data of rock mass surfaces. *Comput. Geosci.* **2022**, *169*, 105241. [[CrossRef](#)]
51. Tang, H.; Song, X.-P.; Zhao, F.A.; Strahler, A.H.; Schaaf, C.L.; Goetz, S.; Huang, C.; Hansen, M.C.; Dubayah, R. Definition and measurement of tree cover: A comparative analysis of field-, lidar- and landsat-based tree cover estimations in the Sierra national forests, USA. *Agric. For. Meteorol.* **2019**, *268*, 258–268. [[CrossRef](#)]
52. Sithole, G.; Vosselman, G. Experimental comparison of filter algorithms for bare-Earth extraction from airborne laser scanning point clouds. *ISPRS J. Photogramm. Remote Sens.* **2004**, *59*, 85–101. [[CrossRef](#)]
53. Point Cloud Library. Available online: <https://pointclouds.org/> (accessed on 15 November 2022).
54. CloudCompare Software and Introduction. Available online: <https://www.danielgm.net/cc/> (accessed on 15 November 2022).
55. Terrasolid Software and Introduction. Available online: <http://www.terrasolid.com/home.php> (accessed on 10 November 2022).

**Disclaimer/Publisher’s Note:** The statements, opinions and data contained in all publications are solely those of the individual author(s) and contributor(s) and not of MDPI and/or the editor(s). MDPI and/or the editor(s) disclaim responsibility for any injury to people or property resulting from any ideas, methods, instructions or products referred to in the content.